M. Ahmer Wadee
Department of Civil and Environmental Engineering,
Imperial College of Science, Technology and Medicine,
South Kensington Campus,
London SW7 2AZ, UK

L. A. P. Simões da Silva
Departamento de Engenharia Civil,
Universidade de Coimbra Polo II,
Pinhal de Marrocos,
3030-290 Coimbra, Portugal

Asymmetric Secondary Buckling in Monosymmetric Sandwich Struts

An interactive buckling model for sandwich struts accounting for buckle pattern localization is extended to cover such struts with differing face plate thicknesses. Although this does not affect the critical buckling characteristics of the structure, there is a significant change in the postbuckling behavior; formerly symmetric secondary buckling and imperfection sensitivity characteristics lose this quality as both become asymmetric. [DOI: 10.1115/1.1979513]

1 Introduction

Sandwich construction is a mass efficient structural form used extensively in astronautic [1], aeronautic [2,3], and marine applications [4]. They are used as members for general loading situations: bending, shear, and axial loading. In axial compression, however, there are serious structural integrity issues precisely because of their inherent efficiency; their susceptibility to highly unstable interactive buckling phenomena in practical situations is widely accepted [5,6]. Previous work developing a nonlinear variational model, accounting for the severe interaction between overall (Euler-type) and local modes of buckling that leads to highly unstable localized buckling [7], has identified the problems with using orthotropic core materials [8], and with having preexisting defects in terms of lack of straightness in the face plates [9] and face-core delamination [10,11]. These effects do not significantly affect the linearly evaluated critical load capacity, which have been historically well understood [12], but they can have severe implications on the postcritical load-carrying capacity of the sandwich strut concerned. Moreover, the nonlinear effects can seriously question the practical value of linear eigenvalue analysis for these cases—the maximum capacity of the structural component being well below the linearly evaluated critical load and therefore significant factors of safety would need to be applied in relevant design rules.

A further enhancement to this sandwich structure model is presented in this paper where the stiff face plates now have the possibility of having differing thicknesses, hence, introducing a degree of monosymmetry in the cross section [13], which is a common way of modeling corrugated sandwich panels in industrial buildings. Comparing the critical buckling behavior of an Euler strut with a doubly symmetric cross section against a monosymmetric one, it is well known from classical work [14] that the respective levels of the linear buckling load may differ but their postbuckling behavior would still be symmetric, assuming of course that there is no possibility of local buckling within the cross-section itself. However, and here lies the key point, if local buckling is possible then the situation changes significantly; any local buckling on one side of the cross-sectional neutral axis will differ markedly from the other side due to the different configuration of the section on either side of the neutral axis. For the sandwich structure, if the face plates have different thicknesses then this introduces the possibility of the local mode of one of the face plates interacting with the overall mode of buckling in differing degrees depending on the initial sign of the critical mode. The result of this is that although the primary postbuckling response is still symmetric—given that the overall mode of buckling is the first instability—further deformation introduces a second instability that leads to localized buckling in the face plate with greater compression; the magnitude of overall buckling displacement required to trigger the second instability relating to the thickness of the face plate in more compression. The result of this is an asymmetric postbuckling response following the second instability with the consequent imperfection sensitivity also becoming asymmetric.

The present paper begins with the development of the interactive buckling model with the new feature of cross-section monosymmetry. The formulation is based on the variational principle of minimum potential energy, the contributions being from the bending and compression in the face plates, shearing and transverse compression in the core, and the work done by the external load. The equilibrium equations are then developed using the calculus of variations and a linear eigenvalue analysis yields the critical load for overall buckling. As the equilibrium equations form a system of nonlinear ordinary differential equations, subject to integral and boundary conditions, these are solved with a powerful numerical continuation code for a series of different struts with different levels monosymmetry with an objective to determine the severity of the postbuckling response. A particularly severe case is then investigated in detail such that results from both the perfect and imperfect struts, along with a consideration of the worst case imperfection, are presented. Conclusions are then drawn.

2 Interactive Buckling Model

Sandwich panels have stiff face plates placed on a lightweight and softer core material. Figure 1 shows the layout of the sandwich strut to be studied. Face plates are assumed to be thin, which in the present case means that through thickness shear is negligible and that the depth of the core b is large in comparison, isotropic and have a Young's modulus E and Poisson's ratio ν. The core can be constructed from balsa wood, two-dimensional cellular materials such as, aluminium honeycombs, or three-dimensional cellular materials such as polyurethane foams [15–17]. The constitutive law for these materials are commonly assumed to be either isotropic, orthotropic, or transversely isotropic. In the present paper, for the least complexity, the core will be assumed to be homogeneous and isotropic with Young's modulus E_c and Poisson's ratio ν_c, even though previous interactive localized buckling studies have investigated the effect of core orthotropy [8]. The principal difference from previous interactive buck-

Contributed by the Applied Mechanics Division of THE AMERICAN SOCIETY OF MECHANICAL ENGINEERS for publication in the ASME JOURNAL OF APPLIED MECHANICS. Manuscript received by the Applied Mechanics Division March 19, 2004; final revision, December 3, 2004. Associate Editor: E. M. Arruda. Discussion on the paper should be addressed to the Editor, Prof. Robert M. McMeeking, Journal of Applied Mechanics, Department of Mechanical and Environmental Engineering, University of California-Santa Barbara, Santa Barbara, CA 93106-5070, and will be accepted until four months after final publication in the paper itself in the ASME JOURNAL OF APPLIED MECHANICS.

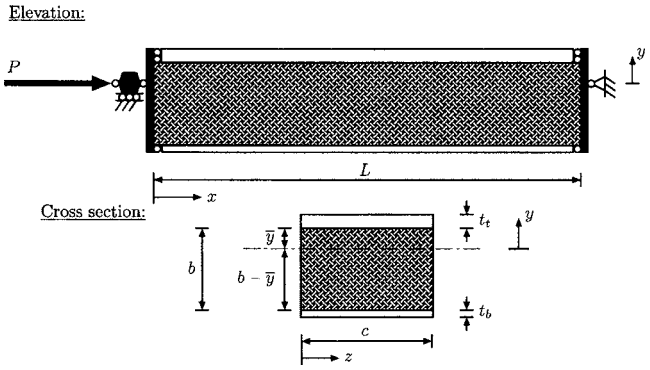

Fig. 1 The sandwich strut and its cross section. The face plates can have different thicknesses (t_b and t_t) and that the distance from the top face plate to the neutral axis is $\bar{y}$. Note that the load P is applied at the neutral axis of the strut.

ling formulations is that here the face plates have differing thicknesses introducing the opportunity for asymmetry of response particularly in the postbuckling range; the symmetry of the critical buckling response is basically unchanged but the relative location of the resulting secondary instability depends on the thickness configuration of the face plates and the initial orientation of the critical buckling displacement. It is also worth noting that owing to face plate anisotropy, monosymmetry can be introduced to the sandwich panel even if face plates have equal thicknesses [18].

The expected behavior of such a strut in compression is for it to follow the pure squash fundamental path, Fig. 2(*a*), and then to buckle in the overall mode—Fig. 2(*b*)—causing differential compression in the faces. This is likely to be followed closely by a secondary bifurcation, in which the face under the greater compression buckles in a second *localized* mode, Fig. 2(*c*). Any initial geometric imperfection in the strut (shown as an initial value of end-shortening $\mathcal{E}_i$) smears out the nonsmooth nature of the perfect equilibrium path shown in Fig. 2(*d*).

2.1 Cross-section Monosymmetry. Figure 1 shows the monosymmetric configuration of the sandwich strut with differing face plate thicknesses t_t and t_b representing the "top" face and "bottom" face, respectively. When undergoing overall buckling, the bottom face plate is deemed always to have the greater compression; the extra secondary buckling displacement is thus always confined to that face plate. With these definitions, the distance of the cross-section neutral axis from the top face-core interface $\bar{y}$ can be found in the conventional way for a section with different material elements and is a key quantity to the formulation of the model

$$\bar{y} = \frac{E_c b^2 + E t_b [2b + t_b(1-\tau^2)]}{2[E_c b + E t_b (1+\tau)]}, \tag{1}$$

where the ratio of the face plate thicknesses τ is defined

$$\tau = \frac{t_t}{t_b}, \tag{2}$$

which at times is referred to as the monosymmetry parameter. Of course if the load were to be applied elsewhere from the neutral axis then the structure would combine bending and compression, a more complicated modeling problem which is beyond the scope of the present study and is left for future work.

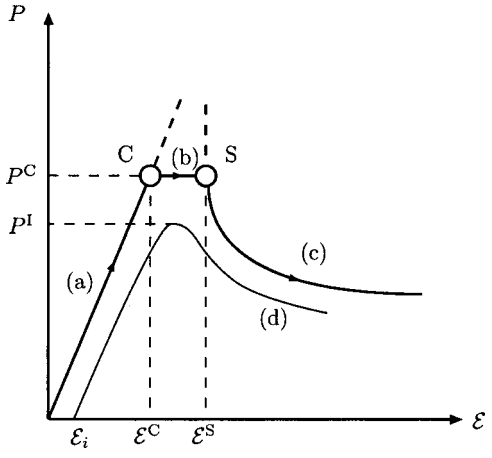

Fig. 2 Typical load P vs end-shortening $\mathcal{E}$ equilibrium diagram for sandwich struts: (a) fundamental path; (b) critical path of overall buckling; (c) secondary path of localized buckling; (d) typical imperfect structure equilibrium path

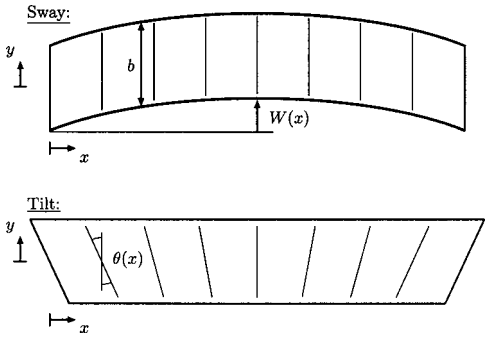

Fig. 3 Sway and tilt components of overall mode

2.2 Face Plate Displacements. An earlier theoretical model [7] had overall buckling represented by sway and tilt components of a long wave mode (Fig. 3) reflecting the possibility of shearing deformations in the core material where

$$W(x) = q_s L \sin\frac{\pi x}{L}, \tag{3}$$

$$\theta(x) = q_t \pi \cos\frac{\pi x}{L}, \tag{4}$$

and interactive localized buckling defined by two functions $w(x)$ and $u(x)$ representing, respectively, lateral and in-plane displacements of a single face plate (Fig. 4). There is also a pure squash strain component of both faces, Δ, which is introduced as a degree of freedom.

3 Variational Formulation

The principle of minimum potential energy is the basis for the following model's formulation. The total potential energy function V is defined as the sum of the internal strain energy stored in the structure (U) minus the work done by the external loads ($P\mathcal{E}$). The accumulated energy has a functional form which is then analyzed using the calculus of variations to determine the equilibrium equations.

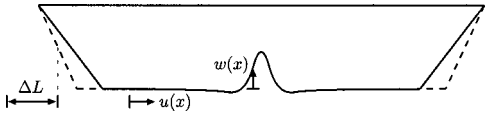

Fig. 4 Displacement functions used to model localized buckling

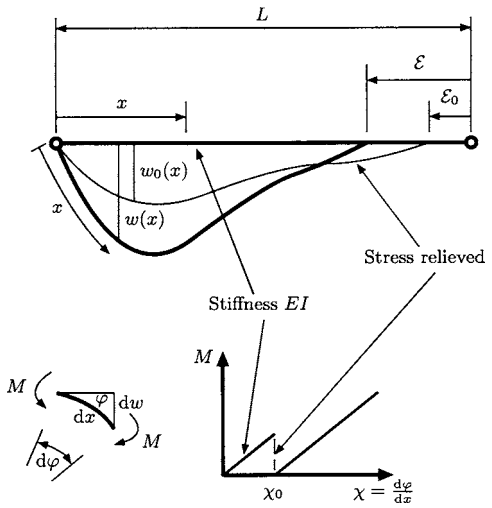

Fig. 5 Stress-relieved state of the strut, after Thompson and Hunt (see Ref. [20])

3.1 Strain Energy. In a general state of deflection there are three components of strain energy U: pure bending in the faces alone (U_b), membrane action in stretching or compressing the faces (U_m), and core energy (U_c) that comprises transverse and shearing strains.

3.1.1 Bending Energy. The bending energy components arise from the overall bending of both faces, coupled with the local bending of the lower face plate. Linear curvature expressions suffice giving the following expression for the contribution from the overall mode:

$$U_{bo} = \frac{1}{2}E\int_0^L \left[(I_t + I_b) q_s^2 \frac{\pi^4}{L^2} \sin^2 \frac{\pi x}{L} \right] dx, \tag{5}$$

where E is the Young's modulus of the face plate with an associated Poisson's ratio ν. The quantities of I_t and I_b are the local minor axis second moments of area of the top and bottom face plates, respectively,

$$I_t = \frac{ct_t^3}{12(1-\nu^2)} \tag{6}$$

$$I_b = \frac{ct_b^3}{12(1-\nu^2)} \tag{7}$$

The model assumes that the bottom face plate has the greater compression once overall buckling has occurred.

The sandwich panel is also modeled with a generalized imperfection that represents the initial deformation of the more compressed face plate w_0, which is formulated from an energy principle. The form of the imperfection closely matches that of the localized buckling mode for the strut on a softening foundation—derived from a first order approximation of a multiple scale perturbation analysis [19]

$$w_0(x) = A_0 \operatorname{sech}[\alpha(x - L/2)] \cos[\beta\pi(x - L/2)/L], \tag{8}$$

where A_0 is the amplitude of the imperfection, with α and β defining the shape of it; α governs the degree of localization and β governs the number of sinusoidal waves in the imperfection. The imperfection is introduced by supposing an initially deformed shape of the more compressed face plate $w_0(x)$ is stress relieved, such that the elemental bending moment, M, and thus stored strain energy of bending U_{bl} drop to zero as represented in Fig. 5 [20,9]:

$$dU_{bl} = \tfrac{1}{2}M d\varphi = \tfrac{1}{2}EI_b(\chi - \chi_0)^2 dx, \tag{9}$$

where χ is the curvature of the strut due to w, χ_0 is the curvature of the strut due to w_0 and EI_b is the flexural rigidity of the imperfect face plate. This also assumes that the strain energy in the foundation is nonzero in the initial state. Assuming a small deflection curvature relationship, i.e., $\chi = w''$, the strain energy of bending becomes

$$U_{bl} = \tfrac{1}{2}EI_b \int_0^L (w'' - w_0'')^2 dx, \tag{10}$$

where primes represent differentiation with respect to the spatial variable x. Therefore the total strain energy stored from bending U_b is the sum of U_{bo} and U_{bl}, thus

$$U_b = \frac{1}{2}E\int_0^L \left[(I_t + I_b) q_s^2 \frac{\pi^4}{L^2} \sin^2 \frac{\pi x}{L} + I_b(w'' - w_0'')^2 \right] dx. \tag{11}$$

3.1.2 Membrane Energy. The membrane strain energy U_m accounts for the axial tension and compression in the face plates when the structure bends after overall buckling. In the "tilt" configuration shown in Fig. 3, the upper face plate simply contributes the tensile equivalent of the compressive strain resulting from overall buckling along with the component of pure squash Δ:

$$\epsilon_{xt} = q_t \frac{\bar{y}\pi^2}{L} \sin \frac{\pi x}{L} - \Delta, \tag{12}$$

while the lower face plate adds as extra contributions the corresponding strains from Von Kármán large-deflection plate theory

$$\epsilon_{xb} = u' + \frac{1}{2}w'^2 - q_t(b - \bar{y}) \frac{\pi^2}{L} \sin \frac{\pi x}{L} - \Delta. \tag{13}$$

The membrane strain energy is therefore ($D = Et_b c/2$):

$$\begin{aligned} U_m &= \frac{Et_c}{2}\int_0^L \epsilon_{xt}^2 dx + \frac{Et_b c}{2}\int_0^L \epsilon_{xb}^2 dx \\ &= D\int_0^L \left\{ q_t^2[\tau\bar{y}^2 + (b - \bar{y})^2] \frac{\pi^4}{L^2} \sin^2 \frac{\pi x}{L} \right. \\ &\quad + 2q_t[b - \bar{y}(1+\tau)] \frac{\pi^2}{L} \sin \frac{\pi x}{L} \Delta + (1+\tau)\Delta^2 \\ &\quad + u'^2 + \frac{1}{4}w'^4 + u'w'^2 - \left[2\Delta + 2q_t(b - \bar{y}) \frac{\pi^2}{L} \sin \frac{\pi x}{L} \right] \\ &\quad \left. \times \left(u' + \frac{1}{2}w'^2 \right) \right\} dx. \end{aligned} \tag{14}$$

3.1.3 Core Energy. In general, the core provides all the transverse and shear resistance but only some of the longitudinal resistance, most of which comes from the faces. Analysis is somewhat simplified if it is assumed that the faces provide all of the latter; a usual assumption if the core is assumed to be *soft* [21]. Plane stress expressions are readily derivable which include a longitudinal strain component in the core, but little is lost conceptually if this is ignored [8]. To match the assumed displacements $w(x)$ and $u(x)$ on the lower face and zero on the upper face of Fig. 4, displacements $w_c(x,y)$ and $u_c(x,y)$ must vary through the core. If x and y are defined as in Fig. 3 and linear variations with y are assumed the following expressions are obtained:

$$u_c(x,y) = \left(\frac{\bar{y} - y}{b} \right) u(x), \tag{15}$$

$$w_c(x,y) = \left(\frac{\bar{y} - y}{b} \right) w(x). \tag{16}$$

It is worth noting that the validity of this assumption has been confirmed in earlier work in a comparative study on a simplified strut on a nonlinear elastic foundation with a simulated overall

buckling mode [7]. Under the assumption that ϵ_x is zero in the core, the remaining core strains can be written

$$\epsilon_y = \left(\frac{\partial w_c}{\partial y}\right) = -\left(\frac{w}{b}\right), \tag{17}$$

$$\gamma_{xy} = \frac{\partial W}{\partial x} - \theta + \frac{\partial w_c}{\partial x} + \frac{\partial u_c}{\partial y} = (q_s - q_t)\pi \cos\frac{\pi x}{L} + \left(\frac{\bar{y} - y}{b}\right)w' - \frac{u}{b}, \tag{18}$$

where G_c is the core shear modulus and can be related to the core's Young's modulus E_c for an isotropic material

$$G_c = \frac{E_c}{2(1+\nu)}. \tag{19}$$

At this point it is worth re-emphasizing that although soft-core materials are usually modeled constitutively as orthotropic or transversely isotropic, the present study takes the simplest case of isotropy such that the effect of differing face plate thicknesses is highlighted more than the constitutive law of the core material; comparisons of core orthotropy versus isotropy have been studied at length in earlier work [8]. Therefore, the general expression for the strain energy stored in the core is

$$U_c = \frac{E_c c}{2(1-\nu_c^2)}\int_0^L \int_{\bar{y}-b}^{\bar{y}} \epsilon_y^2 dy dx + \frac{G_c c}{2}\int_0^L \int_{\bar{y}-b}^{\bar{y}} \gamma_{xy}^2 dy dx, \tag{20}$$

and substituting the appropriate expressions and integrating with respect to y, we obtain ($G = G_c cb/2$):

$$U_c = \int_0^L \left\{ \left(\frac{1}{2}kw^2 - \frac{1}{3}k_1 w^3 + \frac{1}{4}k_2 w^4\right) + G\left[(q_s - q_t)^2 \pi^2 \cos^2\frac{\pi x}{L} + (q_s - q_t)\pi \cos\frac{\pi x}{L}\left(w' - \frac{2u}{b}\right) + \left(\frac{1}{3}w'^2 + \frac{u^2}{b^2} - \frac{1}{b}uw'\right)\right]\right\} dx, \tag{21}$$

where k is introduced as the linear component of the transverse core stiffness

$$k = \frac{E_c c}{(1-\nu_c^2)b}. \tag{22}$$

Note the introduction of nonlinearities in the core's transverse stiffness (k_1 and k_2) that account for the general cellular core material response under direct compression. The force versus displacement profile of a cellular core material in direct compression has a distinctive shape in that it is initially linear followed by a plateau where the stiffness can actually drop below zero ($k_1 > 0$) as the microscopic cell walls in the material matrix buckle elastically. Subsequently the material restiffens ($k_2 > 0$) as the cells densify and the material becomes more resistant to further cellular compression [17,22]. For the purposes of the present study, which is to examine the location of the secondary instability and the initial postbuckling response, the core is assumed to behave in a linearly elastic fashion ($k_1 = k_2 = 0$).

3.2 Work Done By Load. The final component of energy to be identified is the work done by the load. The overall tilt mode contributes nothing to the corresponding deflection $\mathcal{E}$ of a load P applied along the neutral axis of the cross section (Fig. 1), while the contribution from the local buckling of a single face scales the total of the end shortening of the face itself by the ratio of the distance to the neutral axis from the top face plate $\bar{y}$ to the depth of the core b. Together with the contributions from pure squash and sway from overall buckling (Fig. 3) this gives the work done as

$$P\mathcal{E} = P\int_0^L \left[\frac{q_s^2\pi^2}{2}\cos^2\frac{\pi x}{L} - \left(\frac{\bar{y}}{b}\right)u' + \Delta\right] dx. \tag{23}$$

3.3 Potential Energy Functional. The total potential energy V of the complete structure is given by the summation of all the strain energy terms: U_c, U_m, and U_b, minus the work done by the load, $P\mathcal{E}$ [23]. This hybrid form of the potential energy involves three degrees of freedom: q_s, q_t, and Δ; and a functional involving the two functions $w(x)$ and $u(x)$:

$$V = \int_0^L \left\{ \frac{1}{2}E\left[(I_t + I_b)q_s^2\frac{\pi^4}{L^2}\sin^2\frac{\pi x}{L} + I_b(w'' - w_0'')^2\right] + D\left\{ q_t^2[\tau\bar{y}^2 + (b-\bar{y})^2]\frac{\pi^4}{L^2}\sin^2\frac{\pi x}{L} + 2q_t[b - \bar{y}(1+\tau)]\frac{\pi^2}{L}\sin\frac{\pi x}{L}\Delta + u'^2 + (1+\tau)\Delta^2 + \frac{1}{4}w'^4 + u'w'^2 - \left[2\Delta + 2q_t(b-\bar{y})\frac{\pi^2}{L}\sin\frac{\pi x}{L}\right]\left(u' + \frac{1}{2}w'^2\right)\right\} + \frac{1}{2}kw^2 + G\left[(q_s - q_t)^2\pi^2\cos^2\frac{\pi x}{L} + \left(\frac{1}{3}w'^2 + \frac{u^2}{b^2} - \frac{1}{b}uw'\right) + (q_s - q_t)\pi\cos\frac{\pi x}{L}\left(w' - \frac{2u}{b}\right)\right] - P\left[\frac{q_s^2\pi^2}{2}\cos^2\frac{\pi x}{L} - \left(\frac{\bar{y}}{b}\right)u' + \Delta\right]\right\} dx \tag{24}$$

The strut width c is a common factor which can be completely eliminated from the model. It is therefore taken as unity for the purposes of numerical solution.

3.4 Linear Eigenvalue Analysis for Overall Buckling. Linear eigenvalue analysis yields the critical load for overall buckling P^C, arising on the pure squash fundamental path F at which $q_s = q_t = w = u = 0$. The potential energy is nondiagonal with respect to q_s and q_t, and so this critical load occurs when the matrix

$$\mathbf{V}_{ij}^F = \begin{pmatrix} V_{ss}^F & V_{st}^F \\ V_{ts}^F & V_{tt}^F \end{pmatrix} \tag{25}$$

is singular, where

$$V_{ij}^F = \left.\frac{\partial^2 V}{\partial q_i \partial q_j}\right|^F. \tag{26}$$

Therefore the critical load for overall buckling is obtained

$$P^C = 2G + \frac{\pi^2 EI_b}{L^2}(1+\tau^3) - \left[\frac{2G^2}{\frac{D\pi^2}{\tau L^2}[\tau\bar{y}^2 + (b-\bar{y})^2] + G}\right], \tag{27}$$

and this expression holds for both positive and negative values of q_s.

3.5 Equilibrium Equations. The integral in Eq. (24) representing the total potential energy of the physical system which must be stationary at equilibrium; the calculus of variations is applied to find this condition. The analysis that follows is a summary of this application of the calculus of variations. Consider the Lagrangian ($\mathcal{L}$) of the form

$$V = \int_0^L \mathcal{L}(w'', w', w, u', u, x)dx. \tag{28}$$

For the system to satisfy equilibrium V has to be stationary. This requires the first variation of V, which is given by the following expression [24]:

$$\delta V = \int_0^L \left[\frac{\partial \mathcal{L}}{\partial w''}\delta w'' + \frac{\partial \mathcal{L}}{\partial w'}\delta w' + \frac{\partial \mathcal{L}}{\partial w}\delta w + \frac{\partial \mathcal{L}}{\partial u'}\delta u' + \frac{\partial \mathcal{L}}{\partial u}\delta u \right] dx. \tag{29}$$

By satisfying the condition $\delta V=0$, the Euler–Lagrange equations give a system of nonlinear ordinary differential equations

$$EI_b w'''' + D\left[2\Delta w'' + 2q_t(b-\bar{y})\frac{\pi^2}{L}\left(\sin\frac{\pi x}{L}w'' + \frac{\pi}{L}\cos\frac{\pi x}{L}w' \right) - 3w'^2 w'' - 2(u''w' + u'w'') \right] + G\left[\frac{u'}{b} - \frac{2}{3}w'' + (q_s - q_t)\frac{\pi^2}{L}\sin\frac{\pi x}{L} \right] + kw = EI_b w_0'''', \tag{30}$$

$$D\left[u'' + w'w'' - q_t(b-\bar{y})\frac{\pi^3}{L^2}\cos\frac{\pi x}{L} \right] + \frac{G}{b}\left[\frac{1}{2}w' - \frac{u}{b} + (q_s - q_t)\pi\cos\frac{\pi x}{L} \right] = 0. \tag{31}$$

Other equilibrium equations are found by differentiating V with respect to the degrees of freedom Δ, q_s and q_t, respectively,

$$2q_t\pi[b-\bar{y}(1+\tau)] + (1+\tau)\Delta L - \frac{PL}{2D} = \int_0^L \left(u' + \frac{1}{2}w'^2 \right) dx, \tag{32}$$

$$P = E(I_t + I_b)\frac{\pi^2}{L^2} + 2G\left(\frac{q_s - q_t}{q_s} \right) + \frac{2G}{q_s \pi L}\int_0^L \cos\frac{\pi x}{L}\left(w' - \frac{2u}{b} \right) dx, \tag{33}$$

$$\frac{D}{G}\left\{ q_t[\tau\bar{y}^2 + (b-\bar{y})^2]\frac{\pi^2}{L^2} + \frac{4}{\pi L}[b-\bar{y}(1+\tau)]\Delta \right\} - (q_s - q_t) = \int_0^L \left[\frac{2D(b-\bar{y})}{GL^2}\sin\frac{\pi x}{L}\left(u' + \frac{1}{2}w'^2 \right) + \frac{1}{\pi L}\cos\frac{\pi x}{L}\left(w' - \frac{2u}{b} \right) \right] dx. \tag{34}$$

The system of equilibrium equations are also subject to three boundary conditions at each end, these are determined from integrating V by parts and yield the following [7]:

$$w(0) = w''(0) = 0, \tag{35}$$

$$w(L) = w''(L) = 0, \tag{36}$$

$$u'(0) + \frac{1}{2}w'^2(0) - \Delta = \frac{P\bar{y}}{Db}, \tag{37}$$

$$u'(L) + \frac{1}{2}w'^2(L) - \Delta = \frac{P\bar{y}}{Db}. \tag{38}$$

However, owing to the symmetry of the structure lengthwise it is easier to solve the equations numerically between $x=0$ and midspan $x=L/2$. The following symmetry condition is therefore imposed at midspan in the numerical code:

$$w'(L/2) = w'''(L/2) = u(L/2) = 0, \tag{39}$$

and because of this the conditions at $x=L$, i.e., conditions given in (36) and (38) are automatically satisfied.

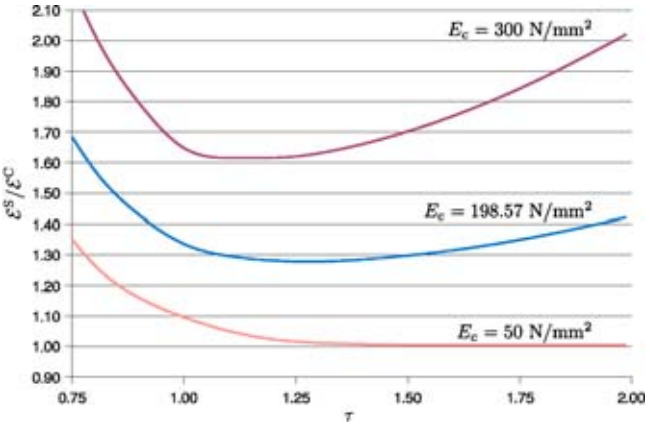

Fig. 6 Relative proximity of secondary and critical bifurcations for struts with different cores and monosymmetries

4 Numerical Experiments

The full system of equilibrium Eqs. (30)–(34) are discretized and solved subject to the conditions (35), (37), and (39) using the numerical continuation package AUTO97 [25]. This allows the evaluation of the physical postbuckling modes and the equilibrium response of a variety of different strut configurations that are selected initially from earlier studies.

In the present study, the initial sign of the overall mode amplitude q_s is of paramount importance; the overall mode is triggered at the same load for both positive and negative values of q_s putting the thicker and thinner face plates into extra compression in turn. Therefore, with a face plate configuration with differing thicknesses, a source of asymmetry in the postcritical buckling response is introduced; the secondary bifurcation that triggers localized buckling occurs at different magnitudes of q_s depending on its initial sign. This leads to the conclusion that the degree of imperfection sensitivity of the strut is asymmetric.

The cases are presented such that a symmetric struts with different core properties are selected from which their relative face plate thicknesses are varied. The struts are compared against each other by measuring the proximity of the secondary instability leading to localized buckling relative to the initial instability that causes overall (Euler-type) buckling. The study then focuses in on a particular strut with a highly pronounced overall-local mode interaction and presents its postbuckling characteristics together with a study of its behavioral sensitivity to initial geometric imperfections.

4.1 Proximity of Secondary Bifurcation. The basic strut used in the numerical study has the following material properties taken from the literature [26,5,7]. The strut length and core depth are kept constant in the present study: $L=508$ mm and $b=50.8$ mm, respectively. The face plate material properties are also kept constant: Young's modulus $E=68{,}947.57$ N/mm^2 and Poisson's ratio $\nu=0.3$. The face plate thicknesses and the Young's modulus of the core are varied in the numerical study.

Figure 6 shows the effect of changing the monosymmetry parameter τ for the strut on the relative gap between the critical bifurcation for overall buckling and the secondary bifurcation for localized buckling ($\mathcal{E}^S/\mathcal{E}^C$). Three different cases of core modulus are shown and it can be seen that the degree of monosymmetry can bring together the separate bifurcations, which in turn results in a less stable structure in the postbuckling range. For the cases of $E_c=300$ and 198.57 N/mm^2, there is clearly a worst case monosymmetry with a minimum value $\mathcal{E}^S/\mathcal{E}^C$ being achieved for a certain value of τ, as shown in Table 1. For the third case, $E_c=50$ N/mm^2, the bifurcations become all but simultaneous for a relatively large range of τ, this is most likely due to the local mode becoming nearly critical for those values.

Table 1 Worst case monosymmetry parameter τ for different core moduli E_c. Simultaneous (compound) bifurcation points would be represented by $\mathcal{E}^S/\mathcal{E}^C=1$.

E_c (N/mm^2)	τ	$\mathcal{E}^S/\mathcal{E}^C$
300	1.15	1.610
198	1.27	1.278
50	1.40–2.00	1.005

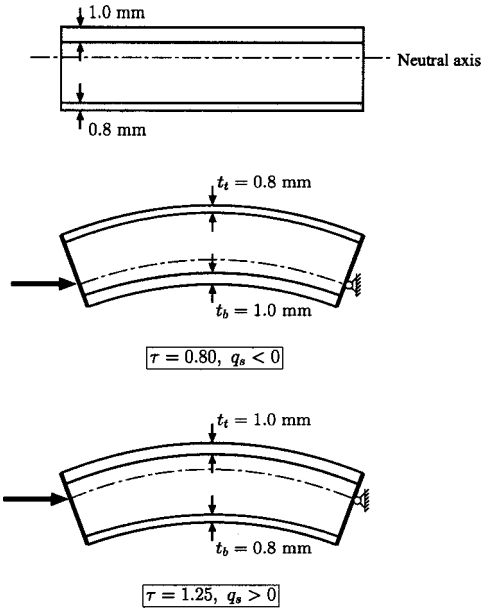

Fig. 7 The selected strut: definitions of the thicknesses t_t, t_b, monosymmetry parameter τ, and the sign of overall buckling q_s

4.2 Full Postbuckling Results. Leading on from the previous section, postbuckling results are now presented for a strut that has quite differing relative secondary bifurcation properties depending on the sign of the overall buckling. Figures 7–9 show a schematic representation of the selected strut, buckling displacements, and equilibrium diagrams for the geometrically perfect strut, respectively. The selected strut has the following dimensions and properties: face thicknesses 1.0 and 0.8 mm; length $L=508$ mm; core depth and properties $b=50.8$ mm, $E_c=50$ N/mm^2, and $\nu_c=0.2$. As shown in Fig. 7, if the thicker face plate is in extra compression after overall buckling is triggered then q_s is negative and if the thinner face plate is in extra compression after overall buckling then q_s is positive. For $q_s<0$ the value of the monosymmetry parameter $\tau=0.8$ with the bifurcation proximity: $\mathcal{E}^S/\mathcal{E}^C=1.267$, and for $q_s>0$ the value of the monosymmetry parameter $\tau=1.25$ with the bifurcation proximity: $\mathcal{E}^S/\mathcal{E}^C=1.016$.

It can be seen in the graphs that the secondary (localized) postbuckling modes of w, shown in Figs. 8(a) and 8(c), have differing localized wavelengths for the face plates. Moreover, the important result from this is shown in Fig. 9 where the proximity between the critical and secondary bifurcations is significant only for $q_s<0$; for $q_s>0$ the gap is much smaller. This implies that if the strut has imperfections forcing $q_s>0$, the strut is much less likely to reach the linear eigenvalue critical load than if $q_s<0$ were forced. This asymmetry in the potential sensitivity to imperfections is now quantified in the following section.

4.2.1 Imperfection Sensitivity. The geometric imperfection w_0, shown in Eq. (8), is introduced for the strut that was selected in the previous section. For each face the imperfection sensitivity for the periodic mode was determined using the following technique: keeping the localization parameter α at zero and the wave number parameter β at the linear eigenvalue solution, the value of the imperfection magnitude $\mathcal{E}_0$, where

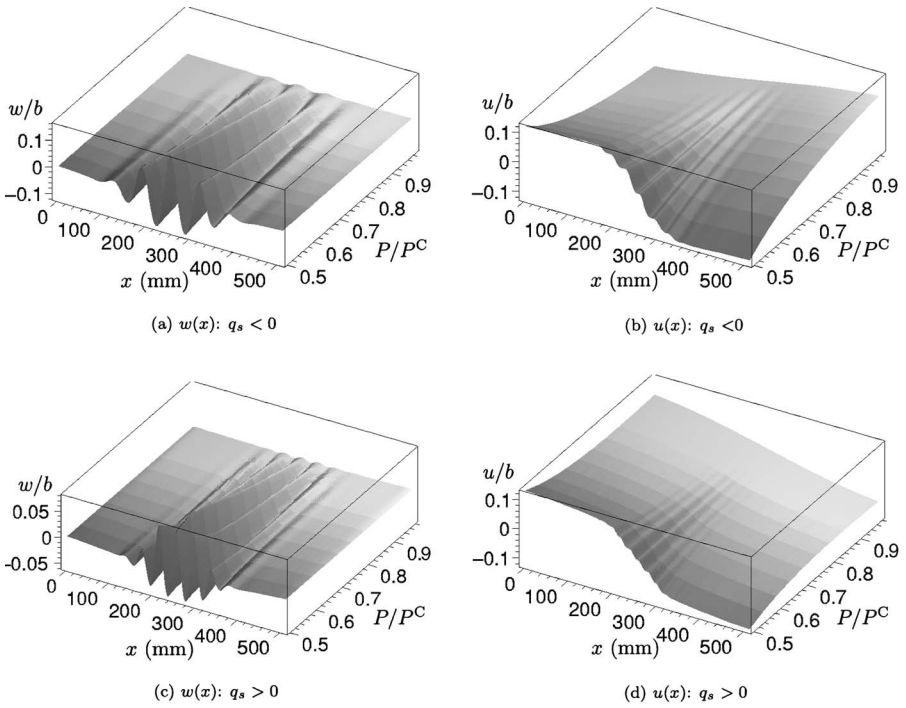

Fig. 8 Postbuckling profiles of monosymmetric strut with face thicknesses 1.0 and 0.8 mm. Other dimensions and properties: $L=508$ mm, $b=50.8$ mm, $E_c=50$ N/mm^2, and $\nu_c=0.2$.

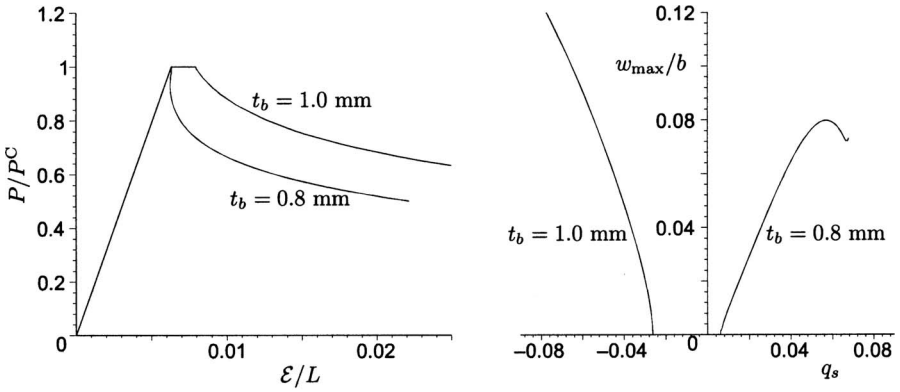

(a) Load vs end-shortening

(b) Localized buckle amplitude vs overall buckle amplitude

Fig. 9 Postbuckling equilibrium diagrams of monosymmetric strut with face thicknesses 1.0 and 0.8 mm. Other dimensions and properties: L=508 mm, b=50.8 mm, E_c =50 N/mm^2, and ν_c=0.2.

$$\mathcal{E}_0 = \int_0^L \tfrac{1}{2} w_0'^2 dx, \tag{40}$$

was varied; each variation of $\mathcal{E}_0$ gave an explicit value of A_0. The imperfection magnitude $\mathcal{E}_0$ is in fact a measure of the axial end-shortening introduced by the imperfection in the face plate prior to the commencement of external loading. The load P was then varied as a parameter in AUTO to find the corresponding limit load P_l/P^C (see Fig. 2). The locus of these values of the limit loads plotted against the size of the initial imperfection defines the so-called imperfection sensitivity curve.

For the localized imperfection at a particular value of $\mathcal{E}_0$, β was still kept at the linear eigenvalue solution but now both α and A_0 were varied. Again, the load P was then varied as a parameter to find the corresponding limit load P_l/P^C; the worst case was defined as the combination of A_0 and α that minimized the limit load for a given value of $\mathcal{E}_0$. Figures 10–12 show the imperfection sensitivity curves and the changing profile of the imperfection respectively for the cases where the sole imperfection is confined to either the thicker or thinner face plate. As expected from previous work [9], the localized imperfection gives the more severely unstable equilibrium response for nontrivial values of $\mathcal{E}_0$. Moreover, the monosymmetry of the sandwich panel means that the relative imperfection sensitivity is higher when the thinner face is imperfect rather than the thicker face; for example, when $\mathcal{E}_0/t_b$ =0.025, the limit load for localized imperfections for $q_s<0$ is P_l/P^C=0.917, the corresponding limit load level for $q_s>0$ being P_l/P^C=0.765, a drop in ultimate strength by 17% for an imperfection amplitude A_0 very much less than a third of the face plate thickness.

5 Conclusions

The present paper has formulated an enhanced variational interactive buckling model for sandwich struts that includes monosymmetry in the cross section, a component type that is relatively common in practical engineering situations. The principal finding is that this monosymmetry of construction introduces asymmetry in the nonlinear response, i.e., different localized postbuckling responses are found depending on the initial orientation of the critical buckling. An important issue here is that the relative proximity between the critical and secondary bifurcation can be significantly changed just by reversing the orientation of the critical buckling mode. The parametric study showed regimes where the degree of monosymmetry forced the critical and secondary bifurcations to be effectively coincident. Moreover, the detailed numerical study that focused in on a particular strut configuration showed a marked difference between the sensitivities to initial imperfections for the individual face plates; the thinner face being much more severely unstable after triggering the interactive (localized) mode than the thicker face.

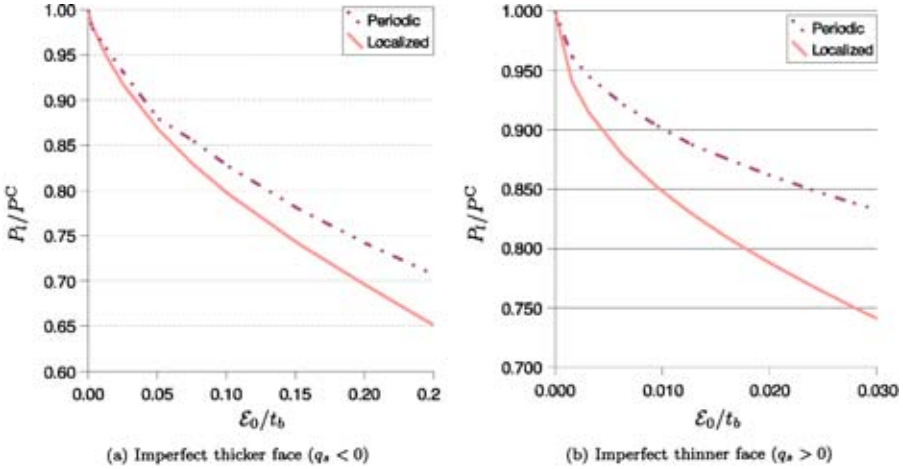

(a) Imperfect thicker face ($q_s < 0$)

(b) Imperfect thinner face ($q_s > 0$)

Fig. 10 Imperfection sensitivity curves for periodic and localized geometric imperfections for the monosymmetric strut with thicknesses 1.0 and 0.8 mm; in this case the thinner face is much more sensitive

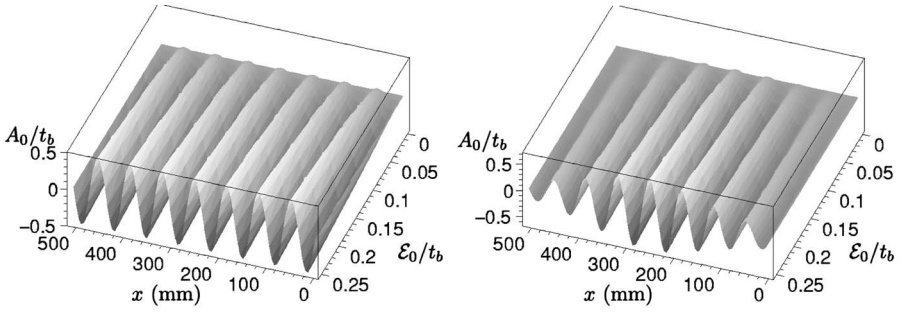

(a) Periodic imperfection (b) Localized imperfection

Fig. 11 Initial imperfection profiles for periodic and worst case localized geometric imperfections for the monosymmetric strut with t_t=0.8 mm and t_b=1.0 mm, i.e., the thicker face buckles (q_s<0)

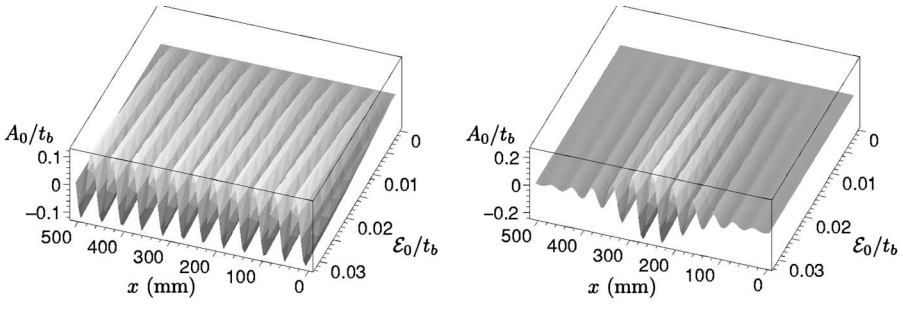

(a) Periodic imperfection (b) Localized imperfection

Fig. 12 Initial imperfection profiles for periodic and worst case localized geometric imperfections for the monosymmetric strut with t_t=1.0 mm and t_b=0.8 mm, i.e., the thinner face buckles locally (q_s>0)

These findings are significant for design practice, as although the basic result of linear eigenvalue analysis is unchanged, the nonlinear analysis reveals a significant sensitivity to very small defects in the geometry such that the structure in certain configurations can only attain a fraction at its critical buckling load.

References

[1] Kodiyalam, S., Nagendra, S., and DeStefano, J., 1996, "Composite Sandwich Structure Optimization with Application to Satellite Components," AIAA J., **34**(3), pp. 614–621.

[2] Bannink, E., Hadcock, R., and Forsch, H., 1978, "Advanced Design Composite Material Aircraft Study," J. Aircr., **15**(10), pp. 661–669.

[3] Duthie, A. C., 1987, "Composite Materials Technology for Helicopters," Plastics and Rubber Int., **12**(1), pp. 20–24.

[4] Knox, E. M., Cowling, M. J., and Winkle, I. E., 1998, "Adhesively Bonded Steel Corrugated Core Sandwich Construction for Marine Applications," Mar. Struct., **11**(4–5), pp. 185–204.

[5] Hunt, G. W., Da Silva, L. S., and Manzocchi, G. M. E., 1988, "Interactive Buckling in Sandwich Structures," Proc. R. Soc. London, Ser. A, **417**, pp. 155–177.

[6] Sokolinsky, V., and Frostig, Y., 1999, "Nonlinear Behavior of Sandwich Panels with a Transversely Flexible Core," AIAA J., **37**, pp. 1474–1482.

[7] Hunt, G. W., and Wadee, M. A., 1998, "Localization and Mode Interaction in Sandwich Structures," Proc. R. Soc. London, Ser. A, **454**, pp. 1197–1216.

[8] Wadee, M. A., and Hunt, G. W., 1998, "Interactively Induced Localized Buckling in Sandwich Structures with Core Orthotropy," ASME J. Appl. Mech., **65**(2), pp. 523–528.

[9] Wadee, M. A., 2000, "Effects of Periodic and Localized Imperfections on Struts on Nonlinear Foundations and Compression Sandwich Panels," Int. J. Solids Struct., **37**(8), pp. 1191–1209.

[10] Wadee, M. A., and Blackmore, A., 2001, "Delamination from Localized Instabilities in Compression Sandwich Panels," J. Mech. Phys. Solids, **49**(6), pp. 1281–1299.

[11] Wadee, M. A., 2002, "Localized Buckling in Sandwich Struts with Pre-Existing Delaminations and Geometrical Imperfections," J. Mech. Phys. Solids, **50**(8), pp. 1767–1787.

[12] Allen, H. G., 1969, *Analysis and Design of Structural Sandwich Panels*, Pergamon, Oxford.

[13] Simões da Silva, L., 1991, "Asymmetric Post-Buckling Behaviour of Two and Three-Layered Sandwich Structures," *Proceedings of the Second Pan American Congress of Applied Mechanics*, Valparaiso, Chile, pp. 494–497.

[14] Timoshenko, S. P., and Gere, J. M., 1961, *Theory of Elastic Stability*, McGraw-Hill, New York.

[15] Easterling, E. J., Harrysson, R., Gibson, L. J., and Ashby, M. F., 1982, "On the Mechanics of Balsa and Other Woods," Proc. R. Soc. London, Ser. A, **383**(1784), pp. 31–41.

[16] Gibson, L. J., Ashby, M. F., Schjaer, G. S., and Robertson, C. I., 1982, "The Mechanics of Two-Dimensional Cellular Materials," Proc. R. Soc. London, Ser. A, **382**, pp. 25–42.

[17] Gibson, L. J., and Ashby, M. F., 1982, "The Mechanics of Three-Dimensional Cellular Materials," Proc. R. Soc. London, Ser. A, **382**, pp. 43–59.

[18] Hohe, J., and Librescu, L., 2004, "Core and Face-Sheet Anisotropy in Deformation and Buckling of Sandwich Panels," AIAA J., **42**(1), pp. 149–158.

[19] Wadee, M. K., Hunt, G. W., and Whiting, A. I. M., 1997, "Asymptotic and Rayleigh-Ritz Routes to Localized Buckling Solutions in an Elastic Instability Problem," Proc. R. Soc. London, Ser. A, **453**(1965), pp. 2085–2107.

[20] Thompson, J. M. T., and Hunt, G. W., 1984, *Elastic Instability Phenomena*, Wiley, Chichester.

[21] Librescu, L., Hause, T., and Camarda, C. J., 1997, "Geometrically Nonlinear Theory of Initially Imperfect Sandwich Curved Panels Incorporating Nonclassical Effects," AIAA J., **35**(8), pp. 1393–1403.

[22] Gibson, L. J., and Ashby, M. F., 1999, *Cellular Solids: Structure and Properties* (Cambridge Solid State Science Series), 2nd ed., Cambridge University Press, Cambridge.

[23] Thompson, J. M. T., and Hunt, G. W., 1973, *A General Theory of Elastic Stability*, Wiley, London.

[24] Fox, C., 1987, *An Introduction to the Calculus of Variations*, Dover, New York.

[25] Doedel, E. J., Champneys, A. R., Fairgrieve, T. F., Kuznetsov, Y. A., Sandstede, B., and Wang, X.-J., 1997, "AUTO97: Continuation and bifurcation software for ordinary differential equations," Technical report, Department of Computer Science, Concordia University, Montreal, Canada; available by FTP from ftp.cs.concordia.cain/pub/doedel/auto.

[26] Brush, D. O., and Almroth, B. O., 1975, *Buckling of Bars, Plates and Shells*, McGraw-Hill, New York.